J. Fluid Mech. (1994), *vol.* 276, *pp.* 163–187

Convective instability in ammonium chloride solution directionally solidified from below

By FALIN CHEN, JAY W. LU AND TSUNG L. YANG
Institute of Applied Mechanics, National Taiwan University, Taipei, Taiwan 10764, ROC

(Received 22 September 1992 and in revised form 28 March 1994)

The stabilities of salt-finger and plume convection, two major flows characterizing the fluid dynamics of NH_4Cl solutions cooling from below, are investigated by theoretical and experimental approaches. A linear stability analysis is implemented to study theoretically the onset of salt-finger convection. Special emphasis is placed on the competition between different instability modes. It is found that in most of the cases considered, the neutral curve consists of two separated monotonic branches with a Hopf bifurcation branch in between; the right-hand monotonic branch corresponding to the boundary-layer-mode convection is more unstable than the left-hand monotonic branch corresponding to the mushy-layer mode. We also conducted a series of experiments covering wide ranges of bulk fluid concentration C_∞ and bottom temperature T_B to study the stability characteristics of plume convection. From the measurement of both temperature and concentration of the interstitial fluid in the mushy layer, we verify that during the progress of solidification the melt in the mush is in a thermodynamic equilibrium state except at the melt/mush interface where most of the solidification occurs. The critical Rayleigh number of the onset of plume convection is found to be $R_{cm}^c = 1.1 \times 10^7 \Pi^*$ (see (22)), where Π^* is the permeability of the mush. This relation is believed to be valid up to supereutectic NH_4Cl solutions.

1. Introduction

The directional solidification of ammonium chloride (NH_4Cl) solution cooled from below is of fluid dynamical interest because of both its unique features in thermodynamic properties and the complicated phenomena of the fluid motion occurring during the solidification process. Its thermodynamic properties, such as the low solid fraction of the mush, the large latent heat of fusion, the lack of water of hydration of the crystal, and the steepness of liquidus curve, are quite different from other salts such as sodium carbonate, sodium sulphate, or isopropanol (Huppert 1990). As far as the fluid motion is concerned, several different convective flows have been observed in experiments and some of them are unique compared to the flow of other aqueous solutions. A detailed description of the convective flows of solidifying 26% NH_4Cl solution has been provided by Chen & Chen (1991). Here, we briefly outline the principal flows. At the beginning of solidification, the ejected lighter and cooler fluid is transported upward by salt-finger convection to a certain height, above which the fingers become unstable and degenerate into large-scale bulk motion. Some time later, rising convective plumes sparsely distributed on the plane of the solidification front come directly from the interior of the mush. Following this, the salt-finger convection fades out gradually while the plume convection becomes increasingly prevalent. The number of plumes increases with time at first, reaches a maximum, then decreases. In

this study, we focus on the stability characteristics of salt-finger convection and plume convection, the two major flows dominating the fluid dynamics of the system.

The stability of salt-finger convection has been investigated experimentally by Tait & Jaupart (1989). They increased the viscosity of 28% NH_4Cl solution by including small amount of a hydroxyethylcellulose compound to examine the onset of salt-finger convection. They found this onset to occur largely in the compositional boundary layer above the melt/mush interface (the so-called boundary-layer-mode convection) while the fluid in the mush does not participate in the initial instability. Worster (1992), in a linear stability analysis, considered the onset of instability of a special binary alloy, with buoyancy ratio A (see the definition in §2.1) equal to zero. As a result, he found the onset of convection to be largely confined to the mushy layer (the so-called mushy-layer-mode convection).

Plume convection, owing to its analogy to the freckles of directionally solidified alloys, has attracted relatively much greater attention. Copley *et al.* (1970) attributed the onset of plume convection to the salt-finger convection above the mush. Sample & Hellawell (1984) found that, after plume convection is well established, new plumes can be generated by withdrawing liquid in the vicinity of the freezing front. Fowler (1985) developed a mathematical model to examine the stability of convective flow in the limiting case that no interaction between convection and solidification was involved. In an experimental study of 26% NH_4Cl solution, Chen & Chen (1991) found that plume convection occurs with bottom temperature as high as 11 °C while no plume convection is observed when the bottom temperature is raised to 12 °C. Using the mean value of the porosity determined by the computed tomography, they indicated that the critical Rayleigh number R_{cm}^c (see the definition in (21)) of the onset of plume convection lies within the range 200 to 250. Tait & Jaupart (1992) and Tait, Jahrling & Jaupart (1992), instead of changing T_B as Chen & Chen (1991) did, increased the viscosity of the NH_4Cl solution to investigate the stability of plume convection. They indicated that the onset of plume convection comes immediately after the onset of mushy-layer convection, which occurs when nonlinear salt fingers prevail above the melt/mush interface. The onset of plume convection (or mushy-layer convection) occurs at about $R_{TJ}^p \approx 25$ (see the definition in (23)) (Tait & Jaupart 1992) when T_B is fixed during the experiment and at $R_{TJ}^p \approx 80 \pm 10$ (Tait *et al.* 1992) when T_B decreases gradually. The comparison between the critical Rayleigh numbers of Chen & Chen (1991) and Tait & Jaupart (1992) suffers from the uncertainty of the permeability of the mush at the onset of plume convection, which will be discussed in §3.3.

In the present paper, we investigate the stability of salt-finger convection by a linear stability analysis and that of plume convection by an experimental approach. In the linear stability analysis, we basically follow the analysis of Worster (1992) while considering a wide range of physical parameters particularly relevant to NH_4Cl solutions. In the experiment, four solutions, $C_\infty = 22\%$, 24%, 26% and 28%, are considered and for each solution T_B varies from as low as -30 °C to a temperature at which no plume convection occurs. We measure the evolutions of both temperature and concentration, observe the flow activities and the crystal growth, and determine quantitatively the stability characteristics of both salt-finger and plume convection. Based on these findings, we discuss, amongst other phenomena, the stability characteristics of salt-finger and plume convection, the interaction between the salt-finger and the plume convection, the driving mechanism for plume convection. The linear stability analysis is done in §2, the experimental work is demonstrated in §3, and finally §4 contains the conclusions and discussion.

2. Onset of salt-finger convection – a linear stability analysis

The onset of salt-finger convection during the directional solidification of binary solutions has been investigated experimentally by Tait & Jaupart (1989) and theoretically by Worster (1992). For a 28 % NH_4Cl solution, Tait & Jaupart found that the onset of salt-finger convection is of the boundary-layer-mode instability. Worster, however, in some parameter ranges, argued that the onset of instability is bimodal and the mushy-layer mode is more unstable than the boundary-layer mode. Since these two studies focused on different parameter ranges and, moreover, the mode of salt-finger instability influences the subsequent flows, we thus re-examine this problem in the parameter range particularly relevant to an NH_4Cl solution. We essentially follow the mathematical model developed by Worster while not excluding the possibility of the occurrence of oscillatory convection.

2.1. *Mathematical formulation and method of solution*

The mathematical formulation in this section is the same as that in Worster (1992), to which the reader is referred for details. For the convenience of subsequent discussions, we briefly outline the mathematical model in the following. We consider a mushy layer that lies above a solid region and below a semi-infinite fluid region. A binary solution of concentration C_∞ and temperature T_∞ is solidified from below and both the melt/mush and mush/solid interfaces move upwards with a constant velocity V. The mushy layer extends from $z = 0$ to $z = h(x, y, t)$, where x and y are the two horizontal axes of a Cartesian coordinate system, t is the time, and h is the position of the melt/mush interface to be determined as part of the solution. The temperature at the mush/solid interface is fixed at the eutectic temperature T_E.

Two sets of equations are required to describe the fluid motion of the system. Each set consists of the conservation of mass, momentum, heat, and solute. Associated with the boundary conditions on both the melt/mush and mush/solid interfaces and the far-field boundary in the melt, these equations can be linearized by the small-disturbance quantities based on the motionless basic state. After applying the normal mode analysis, the linear perturbation equations are obtained as follows. In the fluid region, $z > h$, the disturbance equations are

$$[\mathrm{D}^2 + \mathrm{D} - \omega - \alpha^2]\,\theta = \theta_b' W, \tag{1}$$

$$[\epsilon \mathrm{D}^2 + \mathrm{D} - \omega - \epsilon\alpha^2]\,\Theta = \Theta_b' W, \tag{2}$$

$$(\mathrm{D}^2 - \alpha^2)\, W = \Omega, \tag{3}$$

$$[\mathrm{D}^2 + (\mathrm{D} - \omega)/\sigma - \alpha^2]\,\Omega = \alpha^2(R_t\,\theta - R_c\,\Theta), \tag{4}$$

where both D and the prime represent the differentiation $\mathrm{d}/\mathrm{d}z$, ω is the frequency of the normal mode, α the horizontal wavenumber, θ the disturbance temperature, W the disturbance vertical velocity, Θ the disturbance concentration, $\epsilon = \kappa_{cl}/\kappa_{tl}$ the Lewis number, Ω the disturbance vorticity, $\sigma = \nu/\kappa_{tl}$ the Prandtl number, κ_{cl} the solute diffusivity of the fluid, κ_{tl} the thermal diffusivity of the fluid, ν the kinematic viscosity, and the subscript b denotes the basic state. The thermal and solute Rayleigh number R_t and R_c in the fluid region are defined as

$$R_t = g\alpha^* \Delta T H^3/(\kappa_{tl}\nu), \quad R_c = g\beta^* \Delta C H^3/(\kappa_{tl}\nu), \tag{5}$$

where g is the gravitational acceleration, α^* the thermal expansion coefficient, β^* the solute expansion coefficient, $H = \kappa_{tl}/V$, $\Delta T = T_L(C_\infty) - T_E$, $\Delta C = C_\infty - C_E$, and $T_L(C_\infty)$ is the liquidus temperature corresponding to C_∞.

In the mushy layer, $0 < z < h$, the final equations are

$$\left\{\mathrm{D}^2+\left[1+\Upsilon\frac{\Lambda-\theta_I}{(\Lambda-\theta_b)^2}\right](\mathrm{D}-\omega)+\frac{2\Upsilon(\Lambda-\theta_i)\theta_b'}{(\Lambda-\theta_b)^3}-\alpha^2\right\}\theta=\frac{\Upsilon\theta_b'}{(\Lambda-\theta_b)^2}\xi+\left(1+\frac{\Upsilon}{\Lambda-\theta_b}\right)\theta_b' W, \tag{6}$$

$$\left[\mathrm{D}^2-\frac{\Pi'(\chi_b)}{\Pi(\chi_b)}\frac{\Lambda-\theta_I}{(\Lambda-\theta_b)^2}\theta_b'\mathrm{D}-\alpha^2\right]W=\alpha^2\Pi_b R_m\theta, \tag{7}$$

$$(\mathrm{D}-\omega)\xi=\theta_b' W, \tag{8}$$

where $\Upsilon = L/c\Delta T$ is the Stefan number, L the latent heat of fusion, c the specific heat, $\Lambda = (C_S - C_\infty)/(C_\infty - C_E)$ the concentration ratio, C_S the concentration of solid, C_E the eutectic concentration, θ_I the basic-state temperature at the melt/mush interface, $\xi = \chi\Theta + \phi\Lambda$ the bulk concentration, χ the porosity, ϕ the solid fraction equal to $1-\chi$, Π the permeability of the mushy zone which is related to the porosity χ by $\Pi = \chi^3$ (Worster 1992) (although in §2.2.1 that a uniform permeability $\Pi = 1$ is considered), and R_m the Rayleigh number for the mushy layer defined as

$$R_m = g\beta\Delta C\Pi^* H/(\kappa_{tl}\nu), \tag{9}$$

in which $\beta = \beta^* - \Gamma\alpha^*$, Γ is the slope of the liquidus curve, and Π^* the reference value of the permeability. (When deriving the above equations, we found that the fourth term on the left-hand side of (6) should be read as $2\Upsilon(\Lambda-\theta_i)\theta_b'/(\Lambda-\theta_b)^3$, instead of $2\Upsilon\Lambda\theta_b'/(\Lambda-\theta_b)^3$ as shown in Worster 1992. Since θ_i in the present study is generally of $O(10^{-3})$, very small compared with $\Lambda \approx O(10)$, this error does not lead to any significant difference to the numerical result of Worster 1992.)

These equations are subject to linearized boundary conditions as follows. At $z \to \infty$

$$\theta = 0, \quad \Theta = 0, \quad W = 0, \quad \mathrm{D}W = 0. \tag{10a–d}$$

At $z = h_b$, where h_b is the unperturbed melt/mush interface position,

$$\theta = \Theta, \quad \mathrm{D}\Theta - \mathrm{D}\theta = \frac{1-\epsilon}{\epsilon}\theta_b'\eta, \quad [W] = 0, \quad \mathrm{D}W = 0, \tag{11a–d}$$

$$[\theta] = 0, \quad [\mathrm{D}\theta] = -\frac{\Upsilon}{\Lambda-\theta_I}\theta_B'\eta, \quad \xi = \theta + \theta_b'\eta, \tag{11e–g}$$

$$\mathrm{D}W_{h_b^-} = -\frac{\beta^* R_m \Pi(1)}{\beta R_c}\left(\mathrm{D}V + \frac{\Omega+\alpha^2 W}{\sigma}\right)_{h_b^+}, \tag{11h}$$

where η is the perturbation to the position of the melt/mush interface, i.e. $h(x, y, t) = h_b + \eta(x, y, t)$, and the square brackets denote the jump of the enclosed quantity across the interface. At $z = 0$,

$$\theta = 0, \quad W = 0. \tag{12a, b}$$

To replace R_t and R_c by R_m, Worster (1992) introduced two new parameters, $A = \Gamma\alpha^*/\beta$ and $\Psi = H^2/\Pi^*$, such that $R_t = A\Psi R_m$ and $R_c = (1+A)\Psi R_m$. Equations (1)–(12) consist of a complex eigenvalue problem

$$F = F(R_m, \alpha, \omega; \theta_\infty, \Lambda, A, \epsilon, \sigma, \Upsilon, \Psi) \tag{13}$$

in which a thirteenth-order ordinary differential equation includes (1)–(4) and (6)–(8) subject to the boundary conditions (10)–(12) except the interfacial condition (11*b*), which is used to compute the perturbed interface position η. We solve this eigenvalue

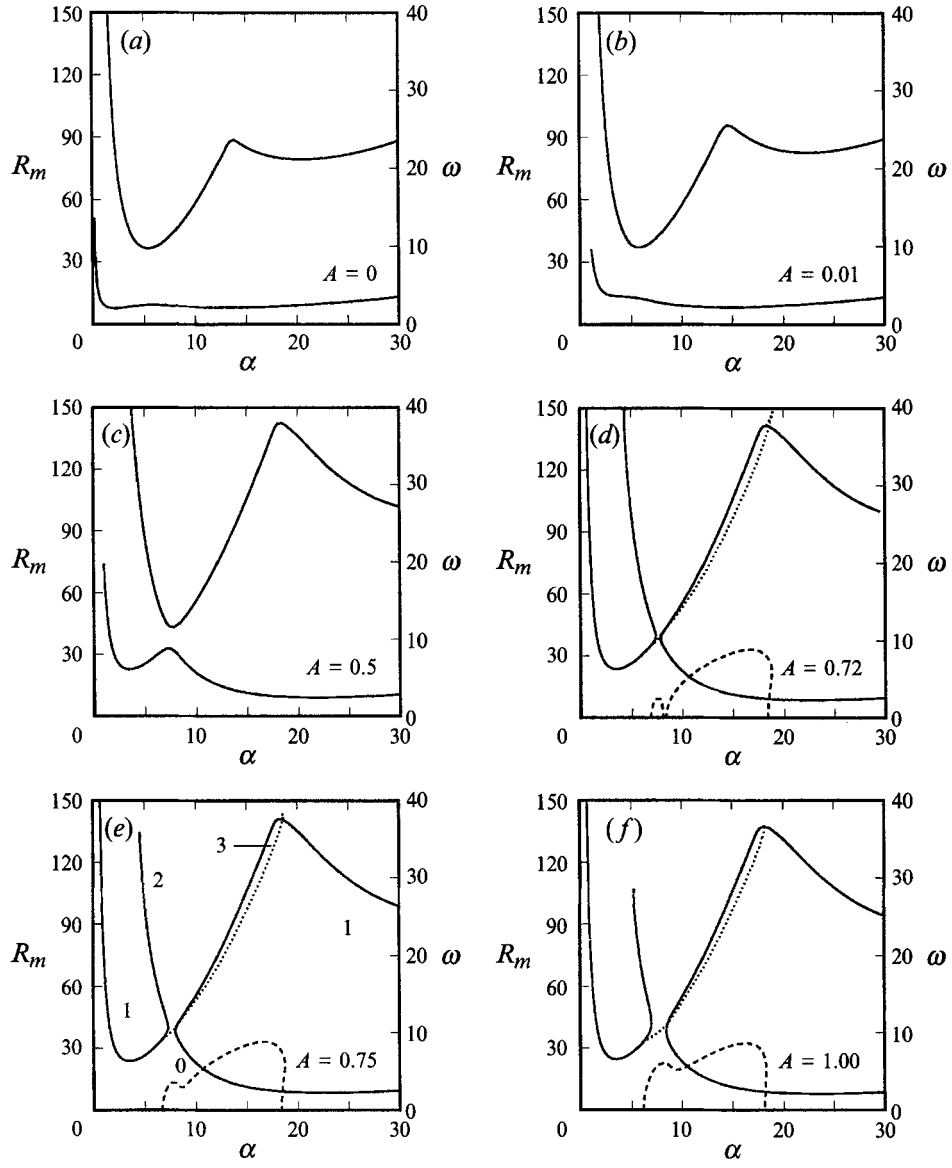

FIGURE 1. Neutral curves for various A when $\theta_\infty = \Upsilon = A = 1$, $\epsilon = 0.025$, $\Pi = 1$, $\Psi = 10^5$, and $\sigma = 10$. The solid curve represents the monotonic branch, the dotted curve represents the oscillatory branch, and the dashed curve shows the value of ω_i. Numbers in (*e*) represent the number of positive ω_r.

problem with a shooting technique. The integration is implemented in a truncated domain (Coriell *et al.* 1980), in which the far-field boundary conditions (10) are imposed at a finite distance z above the melt/mush interface. The value of z is taken sufficiently large ($= 20$ for the present study) so that the integrated results are independent of the value of z. In the mushy layer, since the basic-state temperature is known only implicitly, a change of independent variable proposed by Worster (1992) is used to avoid the need to invert the transcendental equation (see (3.4) of Worster 1992). The resultant boundary-value problem is thus solved by a so-called superposition method developed by Keller (1976), in which an orthonormalization

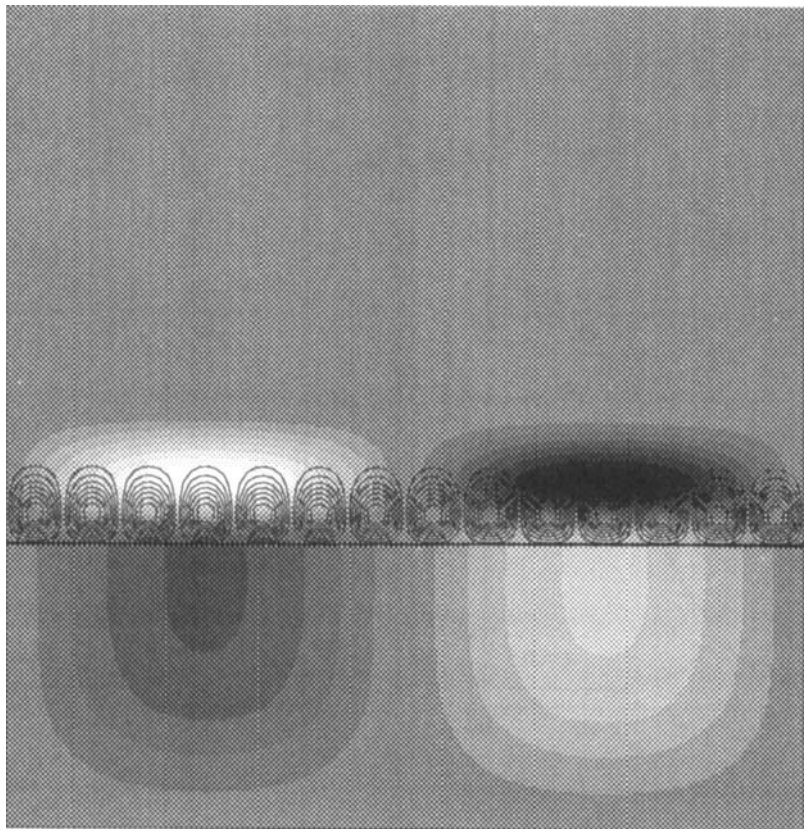

FIGURE 2. The critical boundary-layer mode (solid lines, $\alpha^c = 2.28$, $R_m^c = 8.496$) corresponding to the right-hand branch of the neutral curve of $A = 0.75$, and the critical mushy-layer mode (shadowed, $\alpha^c = 3.49$, $R_m^c = 23.698$) corresponding to the left-hand branch of the same A. The solid line shows the melt/mush interface.

process is imposed to avoid the loss of linear independence of integration. An iteration procedure developed by Powell (1970) is employed to seek the convergence of the eigenvalues R_m and ω.

2.2. *Numerical results*

2.2.1. *Significance of buoyancy ratio A*

Worster (1992) considered the case of $\Upsilon = A = \theta_\infty = 1$, $\sigma = 10$, $\epsilon = 0.025$, $\Psi = 10^5$, $A = 0$, and a uniform permeability $\Pi(\chi) = 1$. His results show that the stability is bimodal and the mushy-layer mode is more unstable. Since $A = 0$ is assumed, the effect due to the interaction between thermal and solutal gradients (double-diffusive) is eliminated from the system, which in fact influences the stability characteristics. We thus reconsider this case for non-zero A and find that A plays a crucial role in determining the mode of instability. Figures 1(*a*)–1(*f*) illustrate a series of neutral curve topologies corresponding to various A. For $A = 0$, figure 1(*a*) shows two marginal curves. The lower curve is virtually the same as that of figure 3 of Worster (1992), which is bimodal and the mushy-layer mode is more unstable. The upper curve is also bimodal and the mushy-layer mode is clearly dominant. As A increases from zero, for example $A = 0.01$ of figure 1(*b*), the boundary-layer mode of the lower curve becomes more unstable while the mushy-layer mode of the upper curve is still more unstable. The two neutral curves move closer (figure 1*c*) as A increases and eventually

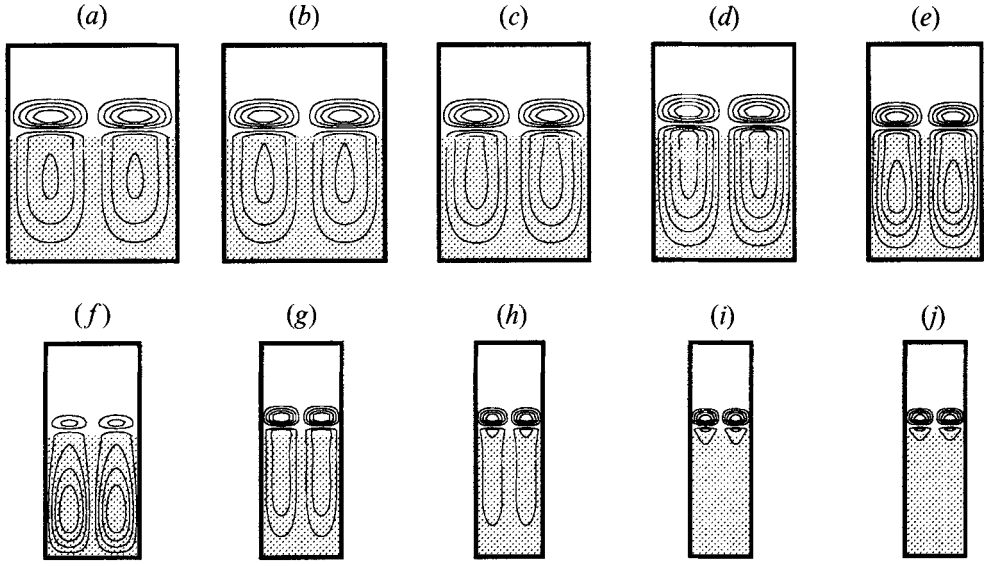

FIGURE 3. The flow patterns of the instability mode along the oscillatory branch of $A = 0.75$. (*a*) $\alpha = 6.68$; (*b*) $\alpha = 7$; (*c*) $\alpha = 7.5$; (*d*) $\alpha = 8$; (*e*) $\alpha = 10$; (*f*) $\alpha = 12$; (*g*) $\alpha = 14$; (*h*) $\alpha = 16.7$; (*i*) $\alpha = 18.7$; (*j*) $\alpha = 18.4$. In these figures, the dotted region represents the mushy zone.

coalesce at $\alpha \approx 7$ when $A \approx 6.9$, where the neutral curve divides into two branches, see figure 1(*d*) for $A = 0.72$. The left-hand branch is the mushy-layer-mode convection and the right-hand branch the boundary-layer-mode convection. A Hopf bifurcation branch which is the dotted line representing the oscillatory mode, connects the two monotonic branches. Another oscillatory branch with higher frequency emerges from the upper part of the right-hand monotonic branch and ends at the same branch. The frequency, shown by the dashed curve, is larger for the oscillatory branch on the right than that between the two branches. The two oscillatory branches will coalesce as A increases further. As shown in figure 1(*e*) for $A = 0.75$, the Hopf bifurcation branch continues to penetrate into the domain enclosed by the right-hand branches and ends at the top. The numbers shown in figure 1(*e*) indicate the number of positive ω_r, which will change by one across the monotonic curve and by two across the oscillatory curve. The frequency of the oscillation has two local maxima, which remain similar as A increases further (see figure 1*f* for $A = 1$).

It is of interest to see the onset flow patterns corresponding to the different modes of instability shown in figure 1(*e*) for $A = 0.75$, which is representative of other A values since it contains all the instability modes. Figure 2 illustrates the two most unstable modes of the two monotonic branches. The mushy-layer mode of the left-hand branch is shown shaded and the boundary-layer mode of the right-hand branch is shown with solid lines, which is the most unstable mode and occurs first in the system. The mushy-layer mode consists of two separated convection cells viscously coupled near the interface (Rasenat, Busse & Rehberg 1989). The boundary-layer mode is largely confined to the melt, sitting in fact just above the melt/mush interface. Note that in figures 2 and 3 for onset flow patterns, the horizontal dimension is scaled on the basis of the mushy-layer height, which is part of the solution of the basic state. Figure 3 illustrates a series of onset flow patterns along the oscillatory curve. At the left-hand end of the curve (figure 3*a*), the onset flow is of the mushy-layer mode. As α increases (up to $\alpha = 10$, see figures 3*b*–3*e*), the viscous coupling remains while the

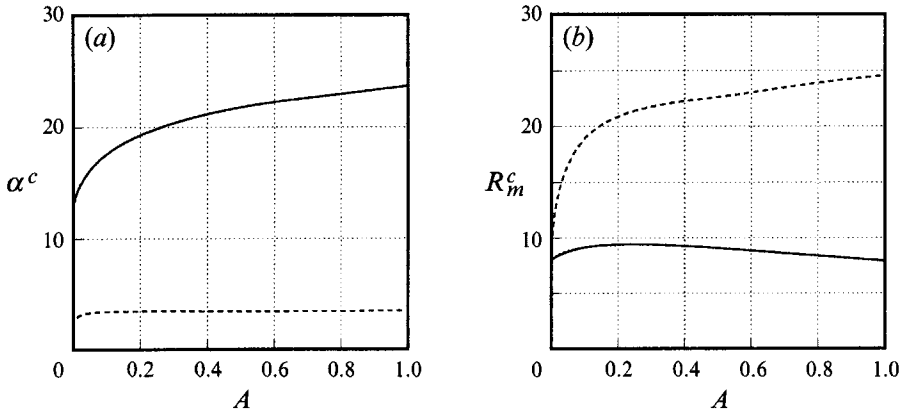

FIGURE 4. The variations of (*a*) α^c and (*b*) R_m^c with A. The solid curve is for the boundary-layer mode and dashed curve for the mushy-layer mode.

convection in the mush increases in strength. For $\alpha = 12$ (figure 3*f*), the convection in the melt becomes very weak whereas the convection in the mush remains strong. As α increases further (figures 3*g*–3*j*), the convection in the melt dominates the system and the convection in the mush virtually vanishes.

To consider the physical meaning of the influence of A on the stability of salt-finger convection, we examine the two modes separately. When A is zero, the mushy layer can be seen as hydrodynamically having zero pressure on the top boundary; as A approaches infinity then the boundary condition at the top becomes one of essentially zero vertical flux. As a result, increasing A stabilizes the mushy-layer mode and the difference in critical Rayleigh number due to these two extremes is approximately a factor of three or less (M. G. Worster, private communication 1993), which is confirmed by the present results shown in figure 4. The influence of A on the boundary-layer mode is more complex. The boundary-layer mode first becomes more stable with increasing A and then becomes less stable as A increases further, which essentially accounts for the stability of the system except at very small A. To see the system as a whole, the net buoyancy is $R_c - R_t = \text{const}[\beta^* \Delta C - A(\beta^*/\Gamma - \alpha^*)\Delta T]$, which shows that any positive A leads to a decrease of net buoyancy thus enhancing the stability of the basic state; namely as A increases from zero, stability is enhanced for both the boundary-layer mode and the mushy-layer mode. The relative effects on these two modes are nevertheless unequal. The mushy-layer mode, as shown in figure 4, becomes more stable relatively to the boundary-layer mode (C. F. Chen, private communication 1994).

2.2.2. *Stability of NH_4Cl solutions cooling from below*

In this subsection, we consider the influence of parameters θ_∞, Λ, Ψ, ϵ and σ on the convective instability in NH_4Cl solutions. Special emphasis is placed on the competition between boundary-layer and mushy-layer modes. The parameters θ_∞ and Λ represent the experimental conditions T_∞ and C_∞, respectively, Ψ (the inverse of Darcy number) accounts for the resistance of the dendritic structure to the flow, and ϵ and σ are the physical properties of the working fluid. The physical properties of ammonium chloride solution needed in the computation are listed in table 1, in which the data particularly relevant to the $C_\infty = 26\%$ solution are shown. In discussing the effect due to each individual parameter, the values of the other parameters are fixed (as shown in table 1). Note that in determining the value of Ψ, we refer to the permeability

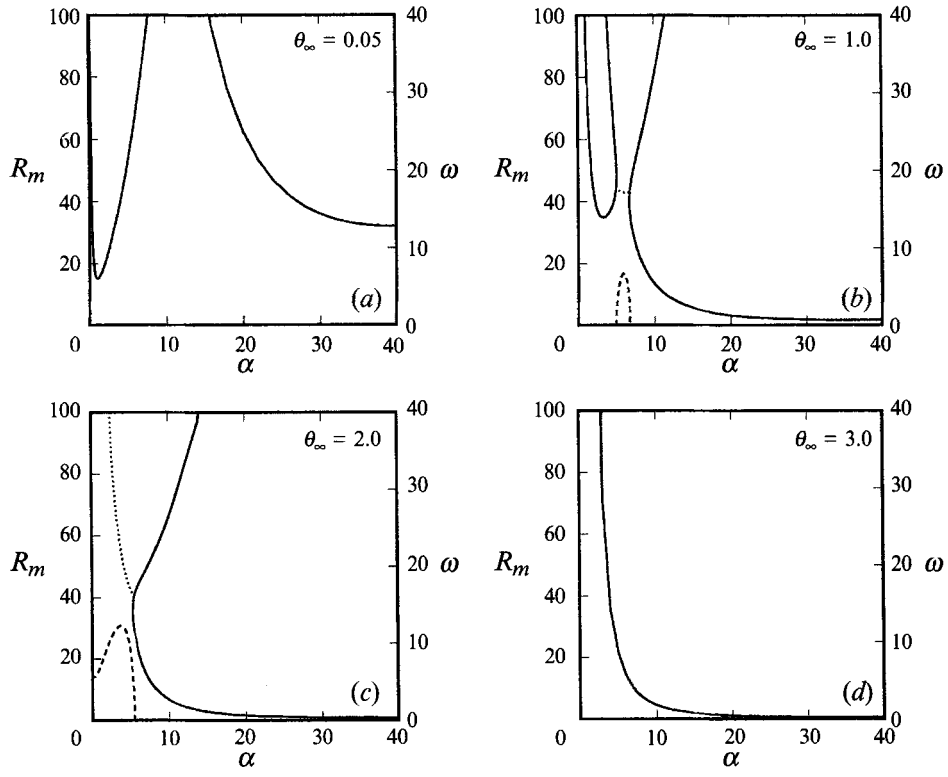

FIGURE 5. Neutral curves for the 26% NH_4Cl solution when $0.3 \leqslant \theta_\infty \leqslant 3$. For description of curves see figure 1.

Γ	4.75 °C %$^{-1}$
L	3.14×10^5 J Kg^{-1}
c	3249 J Kg^{-1} °C^{-1}
κ_{ts}	1.950×10^{-3} cm^2 s^{-1}
κ_{tl}	1.336×10^{-3} cm^2 s^{-1}
κ_{cl}	1.7×10^{-5} cm^2 s^{-1}
κ_{tm}	1.58×10^{-3} cm^2 s^{-1}
κ_{cm}	1.12×10^{-5} cm^2 s^{-1}
ν	1.2×10^{-2} cm^2 s^{-1}
α^*	3.832×10^{-4} °C^{-1}
β^*	2.82×10^{-3} %$^{-1}$
T_E	−15.4 °C
C_E	19.7%
σ	10
ϵ	0.013
A	0.65
Υ	3.20
Ψ	3.5×10^6
θ_∞	0.5
A	12.3

TABLE 1. Physical properties and corresponding dimensionless parameters of 26% NH_4Cl solution

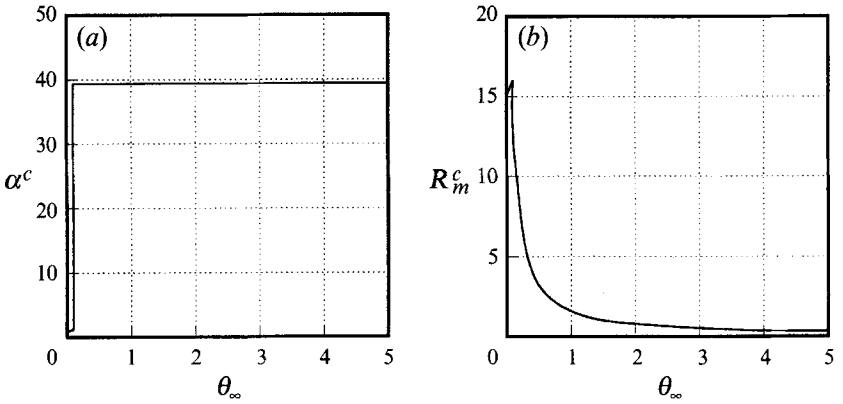

FIGURE 6. The variations of (*a*) α^c and (*b*) R_m^c with θ_∞ for the 26% NH_4Cl solution.

$\Pi^* = 2.41 \times 10^{-5}$ cm^2 determined by Chen & Chen (1991) and the velocity of advance of the melt/mush interface $V = 1.5 \times 10^{-4}$ cm s^{-1} as the height of the mush reaches 1 cm (Chen, Yang & Lu 1993). The non-uniform permeability model $\Pi = \chi^3$ is considered.

(i) *Influence of* θ_∞. We consider $0 < \theta_\infty \leqslant 3$, where for the 26% solution, for instance, $\theta_\infty \approx 0.5$ corresponds to $T_\infty = 30$ °C and $\theta_\infty \approx 3$ to $T_\infty = 75$ °C. Figure 5 shows a series of neutral curve for various θ_∞. For $\theta_\infty = 0.05$ (figure 5*a*) the neutral curve is bimodal and the mushy-layer mode is more unstable. As $\theta_\infty > \theta_\infty^c = 0.1$ (see figure 5*b* for $\theta_\infty = 1$), the boundary-layer mode becomes more unstable and the mushy-layer mode becomes increasingly stable. The neutral curve consists of two monotonic branches and a Hopf bifurcation branch emerging from the left-hand branch and ending at the right-hand branch. For $\theta_\infty = 2$ (figure 5*c*), the monotonic mushy-layer mode virtually vanishes, replaced by the high-frequency oscillatory mode, while the boundary-layer mode dominates the system. For $\theta_\infty = 3$ (figure 5*d*), only the boundary-layer mode exists.

We summarize in figure 6 the variations of α^c and R_m^c with θ_∞. For $\theta_\infty < \theta_\infty^c$, when the mush-layer mode dominates the system, both α^c and R_m^c increase as θ_∞ increases; while for $\theta_\infty > \theta_\infty^c$, the boundary-layer mode dominates, R_m^c decreases as θ_∞ increases whereas α^c remains virtually unchanged. Worster (1992), by focusing on the stability of the mushy-layer mode, predicted that both R_m^c and α^c increase with θ_∞, which agrees with the present result. This, however, does not reflect the reality as the boundary-layer mode dominates the system. To explain physically the influence of θ_∞, we calculated the porosity as well as the mushy layer height of the basic state and found that the averaged porosity increases while the mushy-layer height decrease as θ_∞ increases. The higher porosity leads to a less restrictive porous medium and results in a less stable state; the shallower mushy layer also provides a less restrictive environment and a less stable situation.

(ii) *Influence of concentration ratio* Λ. The value of Λ corresponds to the bulk fluid concentration C_∞. For NH_4Cl solutions, $\Lambda \approx 7$ corresponds to $C_\infty = 30\%$, $\Lambda \approx 12.3$ to $C_\infty = 26\%$, $\Lambda \approx 39$ to $C_\infty = 22\%$, for example. Figure 7 shows a series of neutral curves for various Λ. For $\Lambda = 0.1$ (figure 7*a*) the boundary-layer mode dominates the system and the oscillatory mode prevails in the low-wavenumber domain. The onset flow pattern of these oscillatory modes, as we observe from the eigenfunction variation,

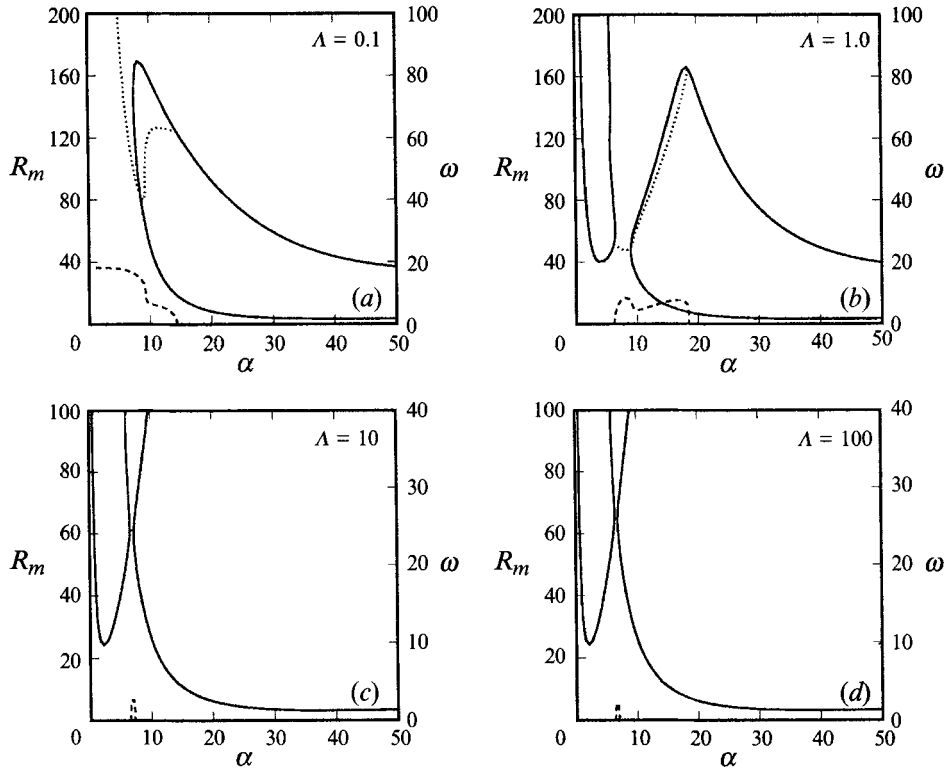

FIGURE 7. Neutral curves for the 26% NH_4Cl solution when $0.1 \leqslant \Lambda \leqslant 100$.

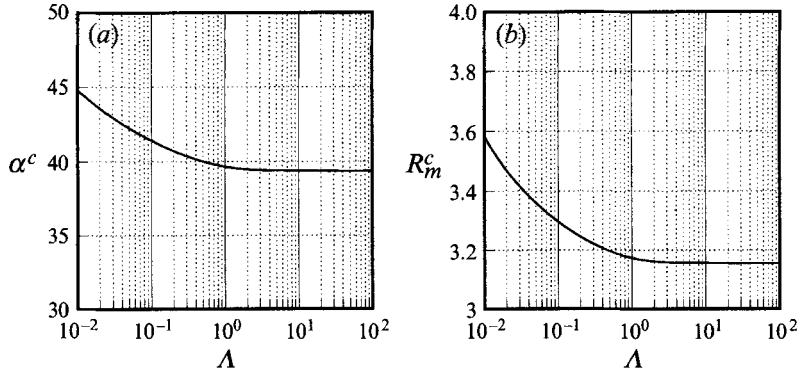

FIGURE 8. The variations of (*a*) α^c and (*b*) R_m^c with Λ for the 26% NH_4Cl solution.

is largely confined to the boundary layer above the interface since at $\Lambda = 0.1$ the porosity of the mush is too small to allow flow motion. As Λ increases (see figure 7*b* for $\Lambda = 1$), the mushy-layer mode becomes increasingly unstable (due to larger porosity) while the boundary-layer mode still dominates. The neutral curve consists of two monotonic branches and an oscillatory branch, which emerges from the left-hand branch, passes through the region enclosed by the right-hand branch and ends at the same branch. For $\Lambda = 10$ (figure 7*c*), the oscillatory branch is between two monotonic branches. For larger Λ (figure 7*d*), the neutral curve remains similar. Figure 8 shows that both R_m^c and α^c decreases with increasing Λ since increasing Λ results in a larger porosity of the mush and thus a less stable state with larger wavelength.

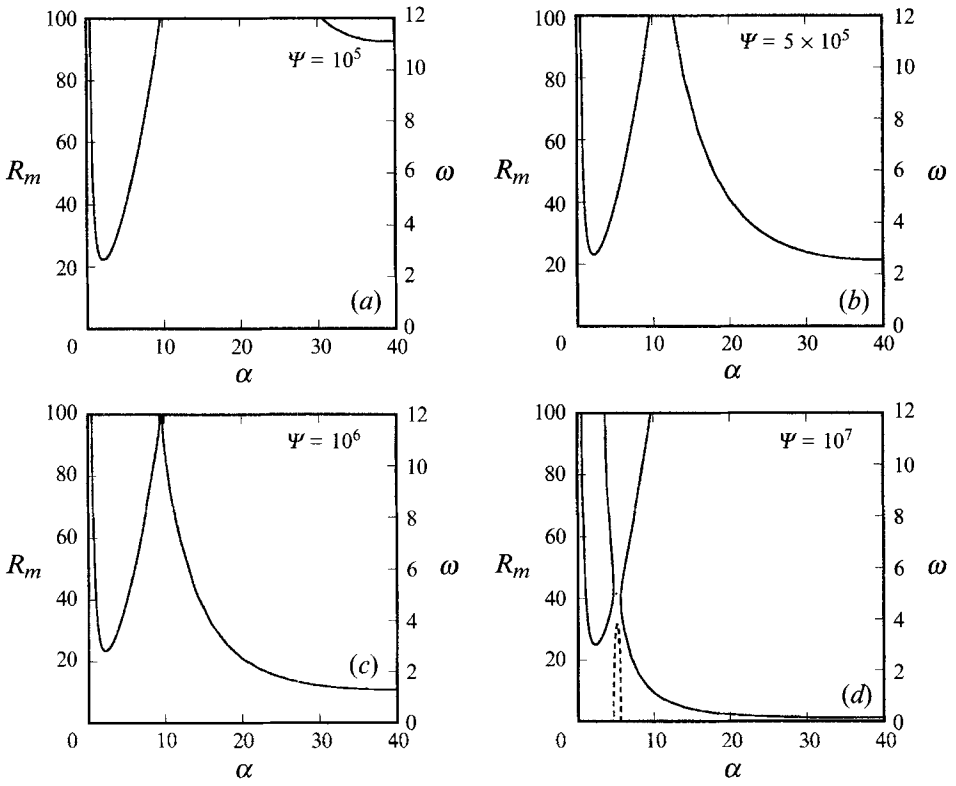

FIGURE 9. Neutral curves for the 26% NH_4Cl solution when $10^5 \leqslant \Psi \leqslant 10^7$.

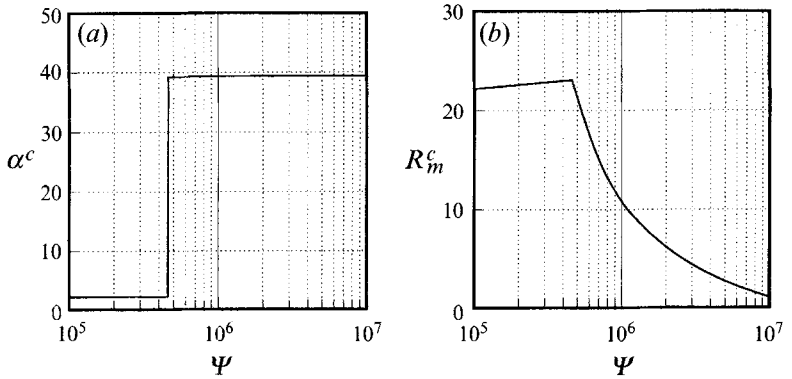

FIGURE 10. The variations of (*a*) α^c and (*b*) R_m^c with Ψ for the 26% NH_4Cl solution.

(iii) *Influence of* Ψ. The parameter Ψ, which by definition is equivalent to the inverse of the Darcy number, accounts for the resistance to the flow in the mush. Accordingly, as Ψ increases, the fluid in the mush will be more stable. Figure 9 demonstrates the topologies of the neutral curves for various Ψ. For $\Psi = 10^5$ (figure 9*a*), the neutral curve is bimodal and the mushy-layer mode is more unstable. When $\Psi > \Psi^c = 4.6 \times 10^5$ (see figure 9*b* for $\Psi = 5 \times 10^5$), the boundary-layer mode becomes more unstable while the stability of mushy-layer mode changes relatively little. As Ψ increases further, the boundary-layer mode becomes increasingly unstable (figure 9*c*). For $\Psi = 10^7$ (figure

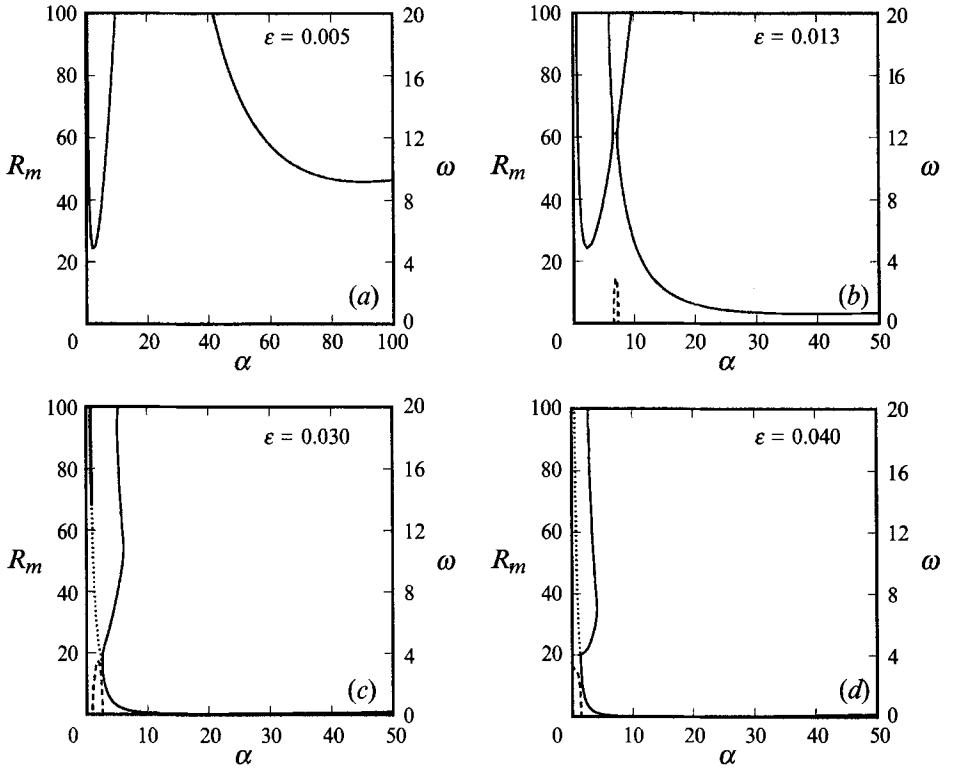

FIGURE 11. Neutral curves for the 26% NH_4Cl solution when $0.005 \leqslant \epsilon \leqslant 0.04$.

9*d*), the neutral curve divides into two branches with an oscillatory branch sitting in between. Figure 10 shows that α^c experiences a dramatic jump at Ψ^c but remains virtually the same for either $\Psi < \Psi^c$ or $\Psi > \Psi^c$. When the mushy-layer mode predominates, R_m^c increases slightly with Ψ due to the smaller permeability in the mush. When the boundary-layer mode dominates, however, R_m^c decreases monotonically with increasing Ψ, because the onset of convection is now largely confined to the boundary layer above the melt/mush interface so that the change of permeability has little effect on the stability of the flow. Nonetheless, according to the definition $\Psi = H^2/\Pi$ and $H = \kappa_{tl}/V$, increasing Ψ may imply an increase of κ_{tl}, which in turn implies a faster diffusion of stabilizing thermal gradient in the melt and thus a less stable state.

(iv) *Influence of Lewis number* ϵ *and Prandtl number* σ. Figure 11 illustrates a series of neutral curve topologies for varying ϵ. For $\epsilon = 0.005$ (figure 11*a*), the neutral curve is bimodal and the mushy-layer mode predominates. As $\epsilon > \epsilon^c = 0.0063$ (see figure 11*b*), the neutral curve divides into two monotonic branches with a Hopf bifurcation branch in between; the boundary-layer mode is now more unstable. As ϵ increases further (figure 11*c*), the mushy-layer mode becomes increasingly more stable while the boundary-layer mode becomes more unstable. For $\epsilon = 0.04$ (figure 11*d*), the mushy-layer mode virtually vanishes, taken over by the oscillatory mode. Physically, increasing ϵ implies an increase of the depth of the compositional boundary layer above the melt/mush interface, which in turn causes the boundary-layer mode to prevail as well as a less stable state, since the thicker boundary layer provides more space for the fluid to convect. Accordingly, for $\epsilon < \epsilon^c$ the mushy-layer mode dominates, and both R_m^c

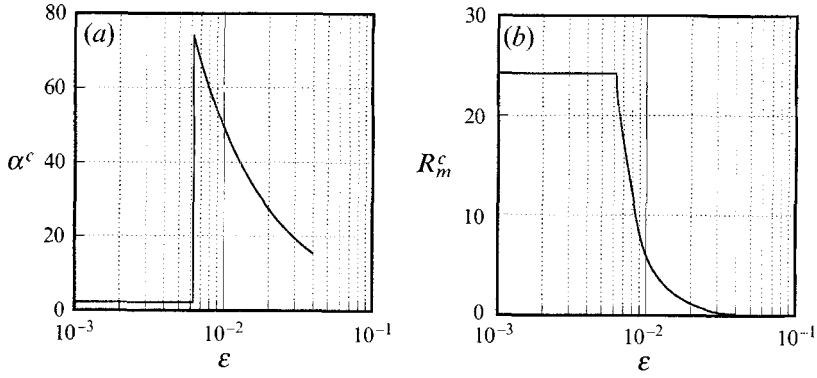

FIGURE 12. The variations of (*a*) α^c and (*b*) R_m^c with ϵ for the 26% NH_4Cl solution.

and α^c remain unchanged with varying ϵ as shown in figure 12 since, as stated above, the ϵ effect is locally confined to the boundary layer above the interface. For $\epsilon > \epsilon^c$ the boundary-layer mode dominates, and both R_m^c and α^c decrease monotonically with increasing ϵ.

With regard to the Prandtl number σ effect, we investigated the neutral curve topologies in $0.01 \leqslant \sigma \leqslant 10$ and found that the neutral curve (not shown) consists of two monotonic branches with a Hopf bifurcation branch in between. The topology remains similar with respect to varying σ. R_m^c, however, decreases generally with increasing σ.

2.3. *Comparison with experimental results*

In an experiment on 28% NH_4Cl solution cooling from below, Tait & Jaupart (1989) added to the solution a small amount of a hydroxyethylcellulose compound, resulting in an increase of fluid viscosity but no change in the phase diagram. By varying the viscosity gradually, they were able to determine the critical condition for the onset of salt-finger convection, a boundary-layer mode convection as they observed. They found the onset of convection to occur when

$$1 < R_{TJ} = g\beta^*(C_\infty - C_I)\, d^3/(\kappa_{cl}\nu) < 8 \tag{14}$$

and $d = \kappa_{cl}/V$. Since their experiment is to some extent relevant to our present linear stability analysis, a comparison between their experimental result and the present theoretical result is thus made in the following.

According to the definitions of R_m and R_{TJ}, we find that

$$R_{TJ}/R_m = \epsilon^2 \Psi(\beta/\beta^*)(C_\infty - C_I)/(C_\infty - C_E), \tag{15}$$

where the relations $d/H = \epsilon$ and $\Psi = H^2/\Pi^*$ have been used. Since the dimensionless concentration of the basic state is $\Theta_b = (C - C_\infty)/(C_\infty - C_E)$, we have

$$\frac{C_\infty - C_I}{C_\infty - C_E} = -\Theta_{bI} = \frac{\epsilon}{1-\epsilon}\theta_\infty, \tag{16}$$

in which the basic-state relation $\Theta_b = \theta_{bI} \exp[-(z - h_I)/\epsilon]$ is considered (Worster 1922, equation (3.3)). As a result, we obtain

$$R_{TJ}/R_m \approx \epsilon^3 \Psi \approx O(1) \tag{17}$$

since, in general, $\theta_{bI} \approx O(1)$, $\beta/\beta^* \approx O(1)$, $\epsilon \approx O(10^{-2})$ and $\Psi \approx O(10^6)$. The present analysis predicts that the value of R_m^c generally lies within 3 and 6 for a 28% NH_4Cl

solution, which agrees nicely with the experimental result. We note that in the present analysis the velocity of both the melt/mush and mush/solid interfaces is assumed to be constant whereas in the experiment both interfaces move with a speed proportional to $1/t^{1/2}$. This difference, in view of the good agreement of the critical Rayleigh number, turns out have an insignificant influence on the stability characteristics of the onset of salt-finger convection.

2.4. *Summary for the onset of salt-finger convection*

The above analysis shows that for NH_4Cl solutions cooled from below the mushy-layer mode can become dominant when $\theta_\infty < 0.1$, or $\Psi < 4.5 \times 10^5$, or $\epsilon < 0.0063$. When $\theta_\infty = 0.1$ the bulk fluid temperature T_∞ is very close to the liquidus temperature $T_L(C_\infty)$, which is generally not the case in the experiment. The Lewis number ϵ of NH_4Cl solutions is also well above ϵ^c. The value of Ψ for the NH_4Cl solutions is however uncertain since no measured permeability at the onset of salt-finger convection is available. The buoyancy ratio A also plays an important role in determining the instability mode. When A is slightly larger than zero, as shown in figure 1, the boundary-layer mode becomes more unstable than the mushy-layer mode. In fact, for most of the aqueous solutions, the value of A is always larger than zero. For instance, $A \approx 0.65$ for NH_4Cl solutions, which causes not only the dominance of the boundary-layer mode but the dividing of the neutral curve and the associated Hopf bifurcation as well. From the above discussion we may infer that for NH_4Cl solutions cooled from below, the onset of salt-finger convection is virtually of the boundary-layer mode.

During computing the above numerical results, we noted that the difficulty in calculating the neutral curve has two causes. First, at high-wavenumbers, usually $\alpha > 30$, the equations become highly stiff so that, in order to maintain the linear independence of integration, the number of iterations increases greatly. Secondly, in calculating the oscillatory neutral curves the convergence of iteration is extremely sensitive to the initial guess of (ω_i, R_m). By and large, the initial guess of ω_i lies within 10% of the final solution. To obtain a point on the monotonic curve for $\alpha > 30$, approximately 250 CPU seconds of CRAY YMP/EL is essential. For a point on the oscillatory curve, about 600 CPU seconds are required, if a good initial guess is made.

3. Onset of plume convection – an experimental investigation

In this section, we investigate the onset of plume convection through a series of experiments covering $22\% \leqslant C_\infty \leqslant 28\%$ and $-30\ ^\circ\text{C} \leqslant T_B \leqslant T_B^c$. Results show that the critical condition for the onset of plume convection has a general relation with the permeability of the mush. The possible value of the permeability is also discussed.

3.1. *Experimental equipment and procedure*

The experiment was performed in a tank with horizontal dimensions $12.5 \times 12.5\ \text{cm}^2$ and a depth of 30 cm. The sidewalls and the top wall of the tank were made of Plexiglas while the constant-temperature bottom wall was made of brass, coated with chromium to avoid the possible chemical reaction between brass and ammonium chloride solution. The tank is placed on another brass plate through which fluid could circulate. To ensure good thermal contact between the bottom of the tank and the circulation plate, Dow Corning silicone heatsink compound was embedded between these two surfaces. A thermistor was inserted into the bottom of the tank to monitor the bottom temperature T_B. The cooler used was a Lauda RK20 constant-temperature circulator, which contained a mixture of ethylene glycol and water. The pumping rate of the

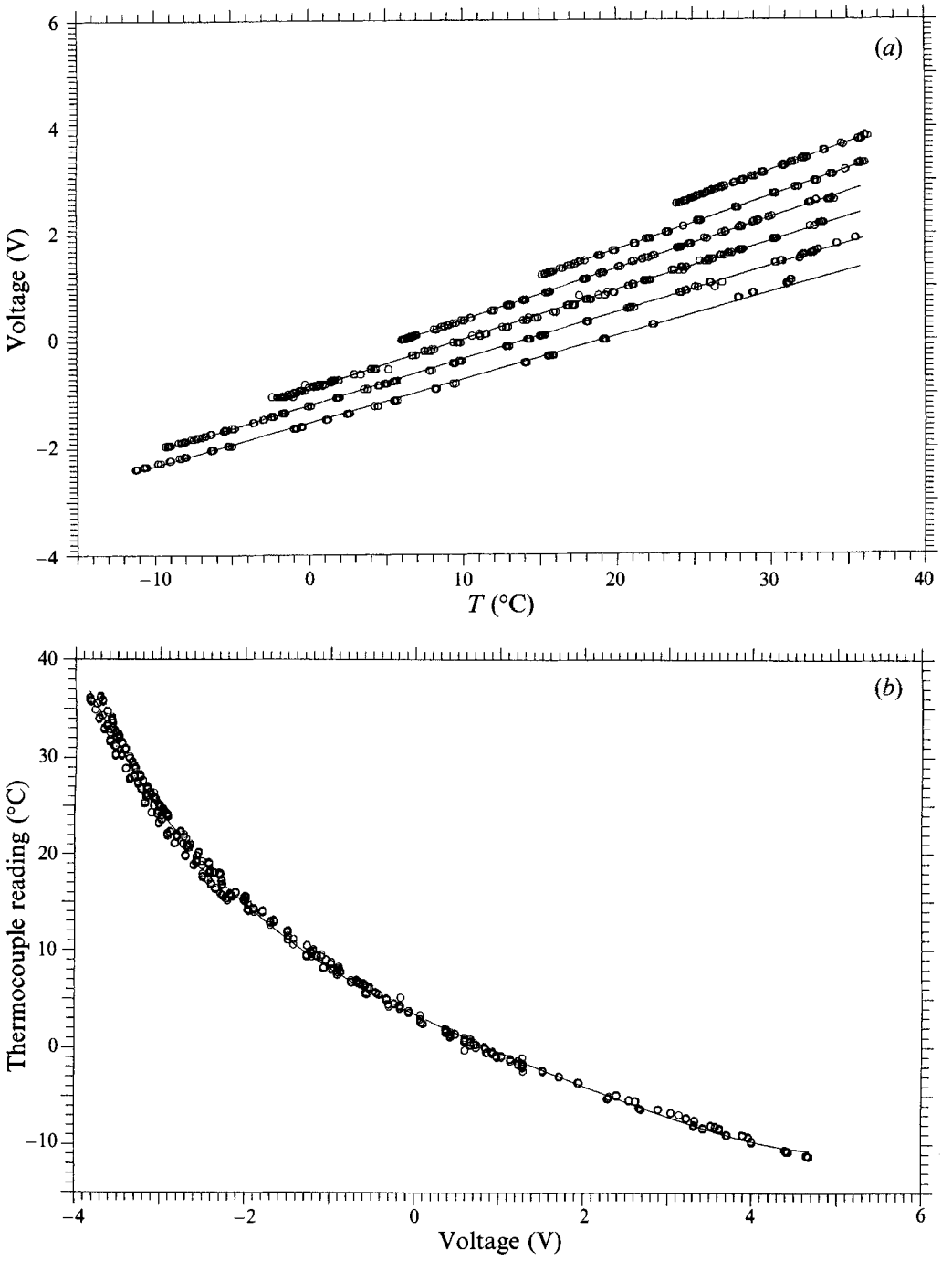

FIGURE 13. Calibration curves for the MSCT probe: (*a*) concentration; (*b*) temperature.

circulator can be up to 4–5 gallon min^{-1} and the fluctuation of the controlled temperature lies within 0.1 °C. During the experiment, the tank was surrounded with styrofoam insulation 4 cm thick except on the front and rear walls where two 4 cm-width slits were provided for observation.

The experiment was started by opening the valve of the cooler to introduce the

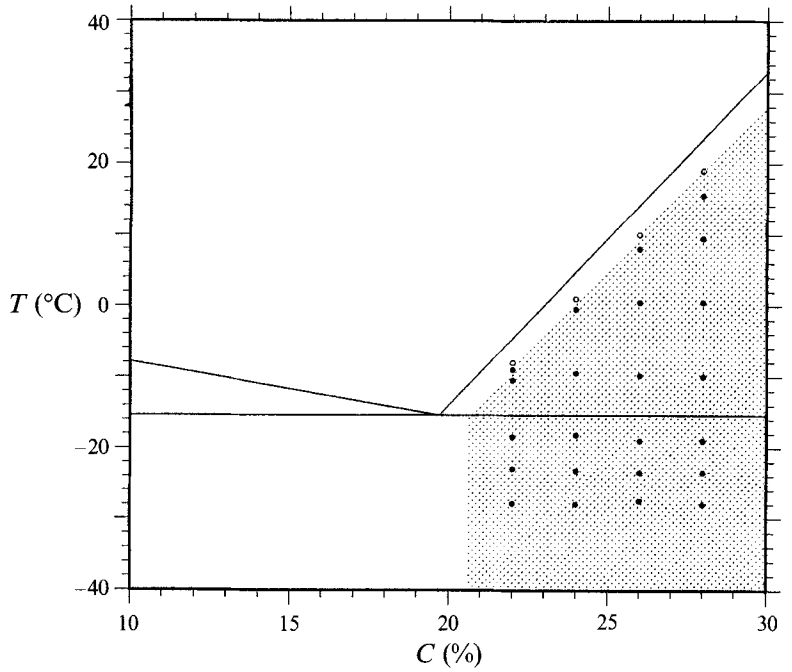

FIGURE 14. The experimental conditions in terms of T_B and C_∞ for the experiments considered and the phase diagram of the NH_4Cl solution: ●, with plume convection; ○, without plume convection. In the experiments in the shaded region plume convection will eventually occur.

coolant with the desired temperature into the circulation plate. The bottom temperature decreased rapidly from the bulk fluid temperature T_∞ and then asymptotically approached the desired value. Typically, it took about 10 minutes to reach a temperature with less than 5% difference from the steady state and about 30 minutes for 1% difference. During the experiment, we observed the growth of the solid and mushy layers from the rear transparent wall, through which the solid and mushy layers can be discerned. The evolution of the flow into the three different types categorized by Chen & Chen (1991) – plume, salt-finger, and bulk circulation – was monitored by the shadowgraph technique.

To detect the evolutions of the concentration and temperature of the fluid in both the fluid and mushy layers, we employed a Micro-Scale Conductivity Temperature (MSCT) probe, which is designed to measure simultaneously the temperature and electrical conductivity of water solutions containing conductive ions (Head 1983). The probe and associated devices provide analogue voltage outputs which are functions of the electrical conductivity and temperature of the solution. The outputs were received by a FLUKE 2289 computer front end and recorded on a hard disc of a personal computer. The data acquisition rate can be up to 0.5–1 Hz and the response time of the probe is less than 0.001 s. After calibrating the probe, we found that the conductivity output is a linear function of both temperature and concentration while the temperature output is an exponential function of temperature and is independent of concentration. We illustrate typical calibration curves for the concentration and temperature of a probe in figures 13(*a*) and 13(*b*), respectively, which can be expressed by

$$C = 18 + \left[v - 1.53\left(\frac{T}{18.6} - 1\right)\right]\left[0.123 + 0.036\left(\frac{T+15}{15}\right)\right]^{-1} \tag{18}$$

for the concentration and

$$T = 3.39 - 4.17v + 0.42v^2 - 0.12v^3 + 0.019v^4 \tag{19}$$

for the temperature. Note that these two relations result in less than 2% error compared with the measured values. In these equations, C is measured as the weight percentage (%) of the solute concentration, T as the temperature in centigrade (°C), and v as the output voltage in volts. According to the design specification, the calibration will shift after about 8 h. In practice, as we noted during the experiment, the calibration shifts by less than 4% after three runs of the experiment, each taking about 6 h or more.

A series of experiments covering wide ranges of T_B and C_∞ were conducted. For a particular C_∞, a T_∞ higher than the liquidus temperature corresponding to C_∞ is required. The experimental conditions in terms of C_∞ and T_B are summarized in the phase diagram of the NH_4Cl solution (figure 14), in which the solid circles represent the experiments with plume convection whereas the open circles represent the experiments without plume convection. The bulk fluid temperatures T_∞ corresponding to the experiments for $C_\infty = 22\%$, 24%, 26% and 28% are, respectively, 23 ± 0.5 °C, 24.7 ± 0.5 °C, 26 ± 0.5 °C, and 29 ± 1 °C. For each case at least two experiments were run although for some of them more than four experiments were carried out.

3.2. *Time evolutions of temperature and concentration*

The MSCT probe was used to monitor both the temperature and concentration evolutions of the fluid at a fixed point as solidification proceeds. Figure 15 illustrates typical measurements for a 26% solution cooled with $T_B = -19.7$ °C. The probe was fixed at 1 cm above the bottom. In this figure and figure 16, the solid curve shows the evolution of concentration, the dashed curve is the evolution of the temperature, and the dotted curve is the calculated concentration related to the corresponding temperature by the liquidus relation

$$T - T_E = \Gamma(C - C_E), \tag{20}$$

where $\Gamma = 4.75$ is the slope of the liquidus. The dotted curve, therefore, represents a thermodynamic equilibrium state for the solution. The calibration of the concentration measurement of the MSCT probe in the mush is difficult because the platinum wire of the probe may be partially or completely surrounded by the growing crystal, which influences the measurement significantly. The voltage output from the probe in the mush therefore cannot reflect the actual concentration of the solution. We thus employed a digital micro-pipetter with a 15 cm long and 0.1 cm diameter hypodermic needle to suck a relevant amount (usually 0.001 l) of the solution at the same depth as the probe's position and ejected the sample onto a refractometer to examine the concentration. The pipetter was mounted on a three-axis stage controller, with which the needle can reach a desired position with a less than 0.01 mm error. We noted that the commercial hypodermic needle is manufactured with a tapered tip, with which the suction from the pipetter collects the solution across a finite depth in the mush. The resultant reading of concentration thus reflects an averaged value over a finite depth instead of a value at the preset point. It is therefore necessary to grind the tip of the needle into a blunt one so that the sample sucked from the tip is the solution at the desired position. In figure 15, two sets of the pipetter measurement are shown as solid and open circles, which were carried out in two different tests whereas the MSCT probe measurement was the result of one of the tests.

It is seen from figure 15 that the probe, placed 1 cm above the bottom, remained in the essentially motionless bulk fluid when $t < 5$ min, where both the concentration and

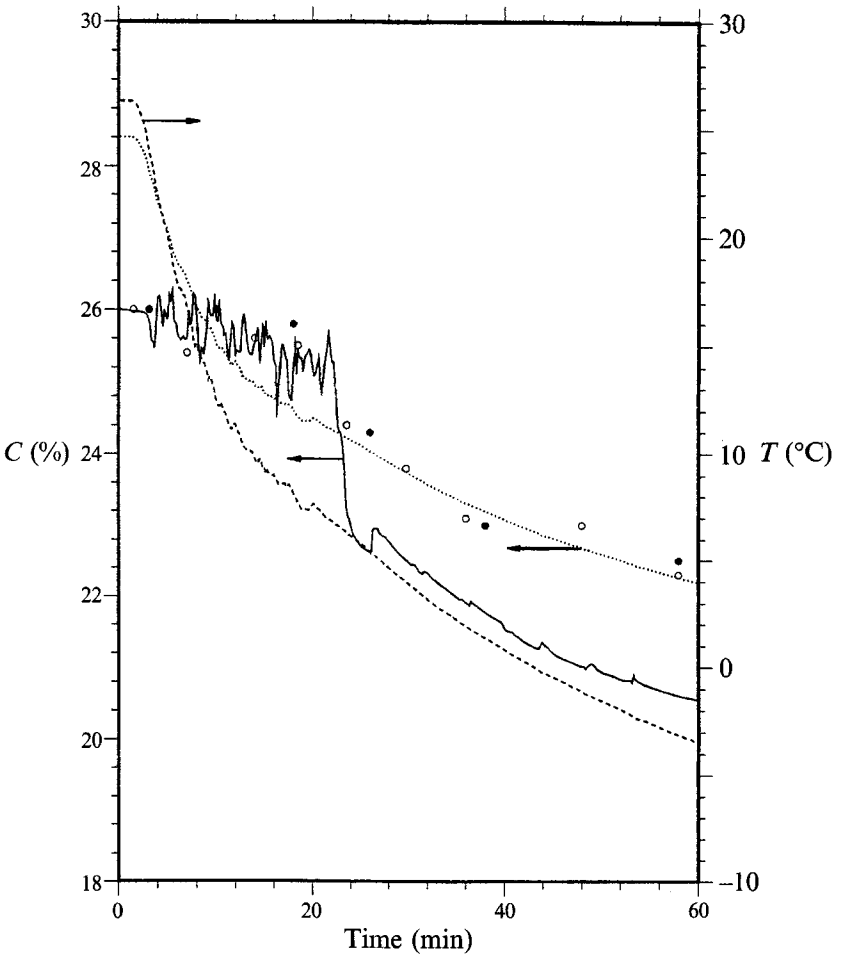

FIGURE 15. Time evolution of the temperature (dashed line), the concentration (solid line, ○, ●) at 1 cm above the bottom when $C_\infty = 26\,\%$ and $T_B = -19.7$ °C. The dotted curve represents the liquidus concentration corresponding to the measured temperature.

temperature remained constant. For $5\text{ min} < t < 22\text{ min}$, the probe entered the turbulent salt-finger convection layer, where the concentration fluctuated significantly, implying that the solution was well mixed due to the turbulent convection, while the thermal gradient was sustained. This suggests that salt-finger convection carries a great deal of mass across the convective layer while the thermal stratification is essentially undisturbed because the buoyancy ratio across the convective layer $[\Delta\rho_c/\Delta\rho_t](\kappa_{cl}/\kappa_{tl})^{1/2}$ is quite small for the present case. At about $t \approx 23$ min, the crystallization front reached the probe, and the concentration experienced a dramatic decrease while the temperature decreased continuously. After entering the mushy layer, the concentration output from the MSCT probe (solid curve) does not reflect the actual value while the temperature reading (dashed curve) is still valid, which was confirmed by the thermocouple calibration. The pipetter measurements, however, should reasonably accurately show the concentration of the melt in the mush.

The dramatic decrease of concentration across the melt/mush interface suggests that a large part of the solidification occurs at the interface, where the melt is supersaturated. In addition, the pipetter measurements of the concentration in the mushy layer indicate

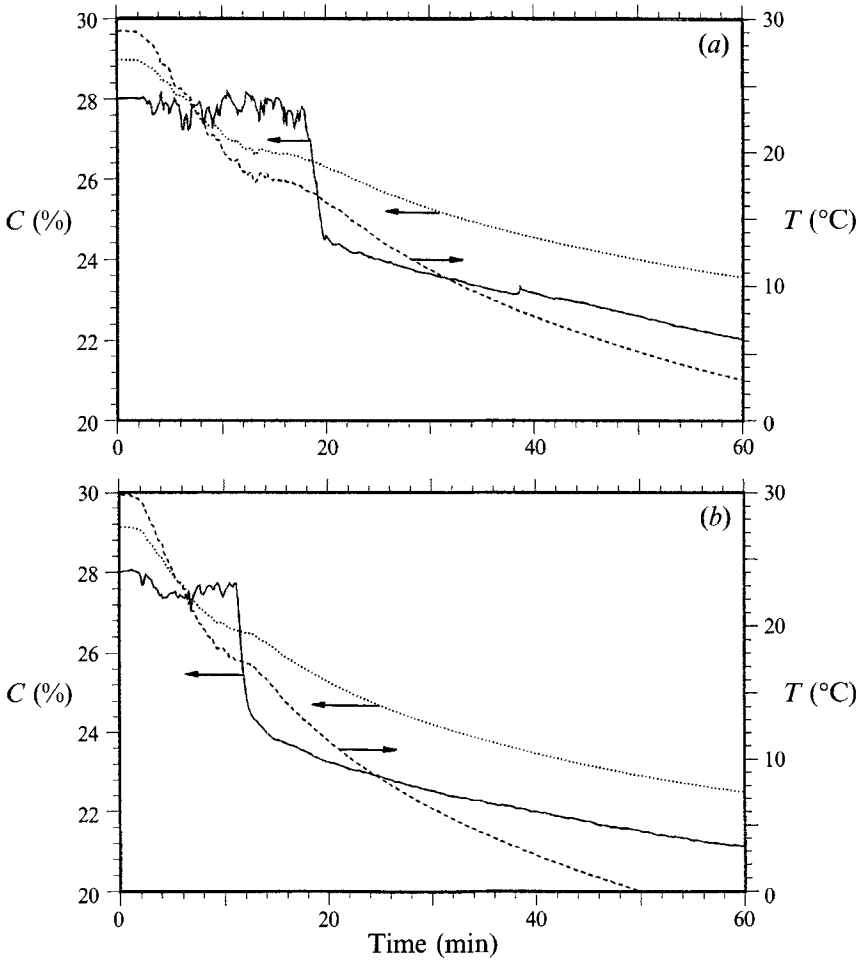

FIGURE 16. Time evolutions of the temperature (dashed line), the concentration (solid line), and the liquidus concentration (dotted line) corresponding to the measured temperature. (*a*) Probe is 1.5 cm above the bottom; (*b*) probe is 1 cm above the bottom.

that the melt in the mush is in a thermodynamic equilibrium state, in which the relation between the concentration and the temperature follows the liquidus relation, (20). Several experiments for different C_∞ and T_B were run and the same conclusion concerning the thermodynamic equilibrium condition in the mushy layer was reached. The thermodynamic equilibrium state reflects the fact that solidification occurs in the mush at a relatively much smaller rate than that at the interface (Kerr *et al.* 1990).

Tait & Jaupart (1989) reported that, with or without salt-finger convection occurring in front of the melt/mush interface, the temperature at the interface is essentially constant as solidification proceeds. This conclusion is also confirmed by the present experiments and will be useful for the subsequent discussion. We show in figures 16(*a*) and 16(*b*) the probe measurements at two different positions, 1.5 cm and 1 cm above the bottom, respectively, for the case of $C_\infty = 28\,\%$ and $T_B = -19.6$ °C. The probe 1.5 cm above the bottom (figure 16*a*), met the interface at about $t = 19.5$ min with the interface temperature T_I about 16 °C. The probe at 1 cm (figure 16*b*), met the interface at about $t = 11$ min when the T_I was about 16.6 °C. The small difference between these two T_I may be due to either the difficulty of precisely locating the interface position,

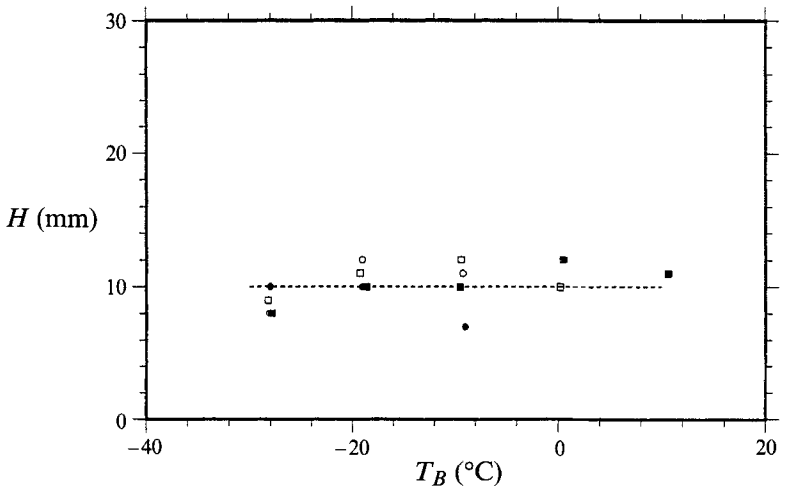

FIGURE 17. The height of the mushy layer at the beginning of plume convection: □, 28%; ■, 26%; ○, 24%, ●, 22%. Each point shows the averaged value over more than two experiments for each case.

which in general is not perfectly flat, or the fact that these two results are obtained from two different experiments, or both. Nevertheless, since the interfacial velocity V depends to some extent upon the supersaturation of the interface, the value of T_I may also change during the experiment because V is changing with time.

3.3. *Critical condition for onset of plume convection*

In the experiment using 26% NH_4Cl solution, Chen & Chen (1991) found that plume convection does not occur when $T_B \geqslant 12$ °C. In addition, at the onset of plume convection, the thickness of the mushy layer is nearly a constant 10 mm in spite of varying T_B. With the assumption that the thermodynamic equilibrium condition holds in the mush (which has been confirmed in §3.2) and with the measurement of the porosity of the mushy layer made by the computed tomography technique, they concluded that the critical solute Rayleigh number across the mush, defined as

$$R_{cm} = \frac{g\beta^* \Delta C_m \Pi^* H_m}{\kappa_{cm} \nu}, \tag{21}$$

for the onset of plume convection lies within 200 and 250. In (21) ΔC_m is the concentration difference across the mushy layer, Π^* the permeability, H_m the thickness of the mushy layer, and κ_{cm} the solute diffusivity of the mush.

In the present study, the experiments were carried out for four solutions with C_∞ ranging from 22% to 28% while T_B varied from about −30 °C to a higher temperature at which no plume convection was observed. These experiments in terms of the experimental conditions C_∞ and T_B are summarized in the phase diagram of the NH_4Cl solution (figure 14). It is found from figure 14 that the critical T_B above which no plume convection occurs is lower than the corresponding liquidus temperature by approximately 4 °C for all C_∞ considered. Moreover, we note that the nearly constant thickness of the mushy layer (about 10 mm) at the onset of plume convection for $C_\infty = 26\%$ also holds for different C_∞ (figure 17). To determine the interface temperature T_I, which is constant during the progress of solidification, the MSCT probe was used to monitor the time evolution of the temperature at 10 mm above the bottom. Results for $C_\infty = 28\%$ with T_B varying from 20 °C to −27.9 °C are illustrated

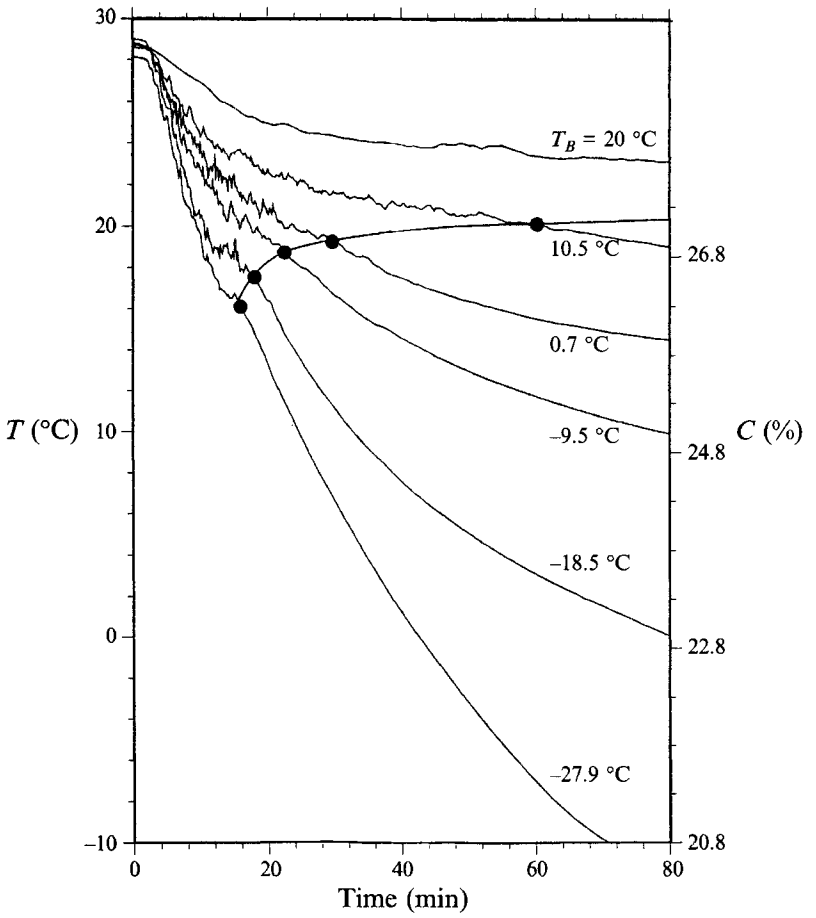

FIGURE 18. Time evolution of the temperature at 1 cm above the bottom for varying T_B when $C_\infty = 28\%$.

in figure 18. The solid circles represent the time at which the probe met the melt/mush interface. Therefore, the curves behind the solid circles include the temperature as well as the concentration evolution in the mush because the thermodynamic equilibrium condition holds. Two vertical scales, T °C and C% related by the liquidus relation (20), are presented in figure 18 for convenience in the mushy zone. From the measurement of the interface temperature T_I (and thus C_I) and the preset T_B, one can obtain the value of ΔC_m across the mushy layer.

We assume that the physical properties of the NH_4Cl solution are constant within the experimental conditions. This assumption is reasonable since, for example, the value of ν changes by less than 2% as C_∞ varies from 28% to 22%, as do the other physical properties of NH_4Cl solutions. The effect of temperature on physical properties within the experimental conditions is also assumed negligible. With these assumptions, as well as the data for ΔC_m and H_m, the critical Rayleigh number of the onset of plume convection and the permeability has the general relation

$$R_{cm}^c = 1.1 \times 10^7 \Pi^* \tag{22}$$

with an uncertainty lying within $\pm 4\%$, which is mainly due to the variation of ΔC_m and H_m. This relation is valid for $22\% \leqslant C_\infty \leqslant 28\%$, and is believed to be also valid for other supereutectic NH_4Cl solutions. If the permeability $\Pi^* = 2.41 \times 10^{-5}$ cm^2

obtained by Chen & Chen (1991) at the end of plume convection is considered, the critical Rayleigh number for the onset of plumes, R^c_{cm}, is approximately 250, below which the plume convection will not occur. If the permeability at the onset of plumes is considered, the R^c_{cm} will be larger than 250 since the permeability in general decreases with time.

Recently, Tait & Jaupart (1992) have experimentally determined the critical condition for mushy-layer-mode convection, equivalent to the plume convection of the present study, by increasing the viscosity of the solution. For a 28% NH_4Cl solution, they found that the onset of plume convection occurs at

$$R^p_{TJ} = \frac{g\gamma_0 \Delta T_m H_0 \Pi_0}{\kappa_{tl} \nu} \geqslant 25, \tag{23}$$

where $\gamma_0 = \rho(\alpha^* - \beta^*/\Gamma)$, when salt-finger convection prevails above the melt/mush interface. In calculating Π_0, they used a permeability model simulating an array of parallel cylinders and considered $\chi = 0.9$, resulting in $\Pi_0 = 2.31 \times 10^{-3}$. The mushy-layer depth at the onset of plume convection was also about 1 cm (see their figure 15 for water). Accordingly, the comparison between R^p_{TJ} and R^c_{cm} is

$$\frac{R^p_{TJ}}{R^c_{cm}} \approx O(10^{-2}) \frac{\Pi_0}{\Pi^*}, \tag{24}$$

in which we note that $(\gamma_0/\beta^*)(\Delta T_m/\Delta C_m) \approx O(1)$ since the liquidus relation holds, $H_0/H_m \approx O(1)$, and $\kappa_{cm}/\kappa_{tl} \approx O(10^{-2})$. By substituting (22) and $R^p_{TJ} = 25$ into the above equation, one obtains that $\Pi_0 \approx 2.3 \times 10^{-4}$, implying that the Π_0 of Tait & Jaupart may be overestimated. The above comparison suggests that, without knowing the actual value of the permeability, (22) should be the most suitable relation to describe the critical condition for the onset of plume convection.

4. Conclusions and discussion

From the theoretical and experimental investigations described, we can draw the following conclusions.

(i) The buoyancy ratio A of the solution plays a crucial role in determining the instability mode at onset. For NH_4Cl solutions, for which $A = 0.65$, the neutral curve is generally divided into two branches, with a Hopf bifurcation in between. The boundary-layer-mode convection generally occurs first, except when the bulk fluid temperature T_∞ is very close to the corresponding liquidus temperature (or $\theta_\infty < 0.1$) or the mush has a large permeability so that $\Psi < 4.6 \times 10^5$.

(ii) During the progress of solidification, crystallization occurs mostly at the melt/mush interface while within the mush there is relatively little crystallization because the fluid in the mushy layer is in thermodynamic equilibrium.

(iii) The onset of plume convection occurs when the mush height is approximately equal to 1 cm and the cooling temperature T_B is about 4 °C lower than the liquidus temperature corresponding to the C_∞ considered.

(iv) The critical R^c_{cm} for the onset of plume convection for a supereutectic NH_4Cl solution can be expressed by (22), a function of permeability. The lowest possible R^c_{cm} is about 250.

Recently, Amberg & Homsy (1993) in a weakly nonlinear analysis of convective flow in a mushy layer indicated that the onset of plume convection is a subcritical instability bifurcating from a motionless basic state due to a finite-amplitude perturbation.

In the experiments, we found that at the onset of plume convection, there was always nonlinear salt-finger convection prevailing above the melt/mush interface. Accordingly, we speculate that the plume convection is a result of the subcritical instability under the perturbation of nonlinear salt-finger convection.

The occurrence of subcritical plume convection (or subcritical mushy-layer-mode convection) due to the nonlinear salt-finger above the mush is understandable if one considers the variation of concentration gradient in the mush. As shown in figure 15, turbulent salt-finger convection efficiently transfers mass between the bulk fluid and the interface while the temperature gradient is relatively unchanged. This turbulent mixing increases the concentration of the fluid near the interface and enhances the concentration gradient in the mush, a destabilizing factor for the mushy-layer mode. The mushy-layer mode is thus triggered by this finite-amplitude disturbance even though the R_{cm} is still much lower than the corresponding one due to small disturbances.

This subcritical instability scenario is also supported by the experiments of Tait *et al.* (1992) and Sample & Hellawell (1984). In one of their experiments, Tait *et al.* gradually reduced T_B, usually 1 °C per 5–10 min, until a desired value was reached. Under such a procedure, the vigour of salt-finger convection increases as T_B decreases. Consequently, the onset of plumes occurred when $70 < R^p_{TJ} \leqslant 90$, almost 3 times larger than that of the case of fixed T_B ($R^p_{TJ} = 25$, see (23)). This result implies that the gradual increase of the vigour of salt-finger convection delays the onset of plume convection since, obviously, the salt-finger convection under low T_B is not strong enough to trigger the convection in the mush. As the salt-finger convection increases in strength and beyond a critical value, plume convection commences under the condition of (22). In their experiment Sample & Hellawell found that new plumes can be generated by withdrawing liquid with a pipette from the vicinity above the interface. This finding is consistent with our speculation that the subcritical bifurcation is triggered by the finite-amplitude velocity disturbance.

With the aid of the above theoretical and experimental investigations, we are able to sketch a clear picture of the convective flow occurring during the solidification process. As the onset of salt-finger convection occurs, the fluid in the compositional boundary layer loses its stability and starts to convect while the fluid in the mush does not participate in the circulation. The salt-finger convection, being largely confined to the boundary layer above the melt/mush interface, becomes increasingly stronger as solidification proceeds. As the mush grows to about 1 cm high, the nonlinear salt-finger triggers the subcritical mushy-layer-mode convection. The upward flow of the convection in the mush carrying colder and less concentrated fluid equilibrates its temperature with the surrounding fluid, causing local re-melting of crystal and in turn driving the formation of a chimney, through which a cold plume is channelled (C. F. Chen, private communication, 1993). The mushy-layer-mode convection circulates between the melt and mush, leading to a decrease of salt-finger convection. The salt-finger convection eventually vanishes and the plume convection solely serves to transport heat as well as mass between melt and mush. The plume convection, after some time, also decays and vanishes at the end of solidification.

The possibility of the occurrence of plume convection in other aqueous solutions cooling from below depends at least on two factors: the vigour of salt-finger convection and the permeability of the mushy layer. As found in a recent experiment of Huppert, Hallworth & Lipson (1993), a small contamination of the solution greatly changes the dendritic morphology and leads to a suppression of plume convection. As also discussed above, Tait & Jaupart (1992) experimentally show that weak salt-finger

convection may not be enough to trigger plume convection. In conclusion, one may expect plume convection to be possible if a vigorous enough salt-finger convection is present along with a mushy layer of large permeability. The determination of the critical salt-finger convective strength and the corresponding permeability may merit future study.

We would like to express our grateful appreciation to Professor C. F. Chen for his valuable comments regarding the experimental results as well as his physical insights into the influence of buoyancy ratio A on the salt-finger stability characteristics, and to Dr M. G. Worster for his suggestions and explanations of the numerical work in many valuable discussions during the visit of F.C. to DAMTP, University of Cambridge, for which the hospitality of Professor H. E. Huppert is also gratefully appreciated. This research has been supported by the National Science Council through Grant No. NSC 80-0401-E-002-26 and NSC 81-F-SP-002-04.

REFERENCES

AMBERG, G. & HOMSY, G. M. 1993 Nonlinear analysis of buoyant convection in binary solidification with application to channel formation. *J. Fluid Mech.* **252**, 79.

CHEN, C. F. & CHEN, F. 1991 Experimental study of directional solidification of aqueous ammonium chloride solution. *J. Fluid Mech.* **227**, 567.

CHEN, F., YANG, T. L. & LU, J. W. 1993 Influence of convection on crystallization of directionally solidified binary solutions. *J. Appl. Phys.* **74**, 7531.

COPLEY, S. M., GIAMEI, A. F., JOHNSON, S. M. & HORNBECKER, M. F. 1970 The origin of freckles in unidirectionally solidified castings. *Metall. Trans.* **1**, 2193.

CORIELL, S. R., CORDES, M. R., BOETTINGER, W. J. & SEKERKA, R. F. 1980 Convective and interfacial instability during unidirectional solidification of binary alloy. *J. Cryst. Growth* **49**, 13.

FOWLER, A. G. 1985 The formation of freckles in binary alloys. *IMA J. Appl. Maths* **35**, 159.

HEAD, M. J. 1983 The use of miniature four-electrode conductivity probes for high resolution measurement of turbulent density or temperature variations in salt-stratified water flows. PhD dissertation, University of California, San Diego.

HUPPERT, H. E. 1990 The fluid mechanics of solidification. *J. Fluid Mech.* **212**, 209.

HUPPERT, H. E., HALLWORTH, M. A. & LIPSON, S. G. 1993 Solidification of NH_4Cl and NH_4Br from aqueous solutions contaminated by $CuSO_4$: the extinction of chimneys. *J. Cryst. Growth* **130**, 495.

KELLER, H. B. 1976 *Numerical Solutions of Two Point Boundary Value Problems.* SIAM.

KERR, R. C., WOODS, A. W., WORSTER, M. G. & HUPPERT, H. E. 1990 Solidification of an alloy cooled from above. Part 1. Equilibrium growth. *J. Fluid Mech.* **216**, 323.

POWELL, M. J. D. 1970 *Numerical Methods for Nonlinear Algebraic Equations* (ed. P. H. Rabinowitz). Gordon & Breach.

RASENAT, S., BUSSE, F. H. & REHBERG, I. 1989 A theoretical and experimental study of double-layer convection. *J. Fluid Mech.* **199**, 519.

SAMPLE, A. K. & HELLAWELL, A. 1984 The mechanism of formation and prevention of channel segregation during alloy solidification. *Metall. Trans.* **15A**, 2163.

TAIT, S., JAHRLING, K. & JAUPART, C. 1992 The planform of compositional convection and chimney formation in a mushy layer. *Nature* **359**, 406.

TAIT, S. & JAUPART, C. 1989 Compositional convection in viscous melts. *Nature* **338**, 571.

TAIT, S. & JAUPART, C. 1992 Compositional convection in a reactive crystalline mush and melt differentiation. *J. Geophys. Res.* **97**, 6735.

WORSTER, M. G. 1992 Instabilities of the liquid and mushy regions during solidification of alloys. *J. Fluid Mech.* **237**, 649.